High strain rate testing of carbon-epoxy laminate crash boxes filled with polymeric cellular 3D-printed cores

International Journal of Impact Engineering 205 (2025) 105401

Contents lists available at ScienceDirect

International Journal of Impact Engineering

journal homepage: www.elsevier.com/locate/ijimpeng

High strain rate testing of carbon-epoxy laminate crash boxes filled with polymeric cellular 3D-printed cores

Francesco Bandinelli [a,*], Alberto Ciampaglia [a], Raffaele Ciardiello [a], Lorenzo Peroni [a], Marco Peroni [b], Martina Scapin [a]

[a] Politecnico di Torino, Department of Mechanical and Aerospace Engineering, Corso Duca degli Abruzzi, 24, 10129, Turin, Italy
[b] European Commission, Joint Research Centre, Ispra, Italy

ARTICLE INFO

Keywords:
CFRP
Crash box
Split Hopkinson pressure bar
3D printing
Cellular structure
Energy absorption
Strain rate

ABSTRACT

In recent years, rising attention has been given to lightweight crash-absorbing composite components. The cost of their realization could be mitigated by the hybridization with 3D-printed cellular infills, limiting the use of high-value materials such as CFRP. The energy absorption capabilities of 3D-printed cellular structures have been proven to be relevant for crash-absorbing applications. In this study, both quasi-static and high strain rate tests are conducted on hybrid crash boxes fabricated by joining an internal 3D-printed infill with an external CFRP reinforcement. A finite element model is developed to reproduce and predict the high strain rate behavior of the structures. Two different internal cellular structures are used as a mold for the hand-layup process of twill carbon-epoxy prepreg, which is applied directly on the 3D-printed surface. Quasi-static tests show that the addition of CFRP to the 3D-printed infill is beneficial for the improvement of the specific energy absorption, with values up to 15 J/g for the maximum reinforced crash box. High strain rate tests show notable differences, highlighting distinct failure and collapse modes, which strongly affect the mechanical properties of the reinforced crash boxes. While unreinforced crash boxes show an improvement of up to 20 % in Specific Energy Absorption (SEA), drops of up to 30 % and 40 % are observed in reinforced crash boxes for Crush Force Efficiency (CFE) and SEA respectively. This suggests that a more appropriate design should be followed to contrast the unfavorable failure and collapse modes observed in impact scenarios.

1. Introduction

In recent years, much effort has been put into lightweight crash-absorbing components for different scopes. Growing attention is given to the reduction of weight in the transportation sector, while passive safety remains a crucial matter [1,2]. In this context, it is of fundamental importance to explore new design possibilities to realize efficient and tunable components for crash-absorbing purposes, such as crash boxes. Crash boxes are energy-absorbing components designed to absorb energy during an impact event. They are specifically engineered to work by axial crushing, with different deformation mechanisms based on their geometry and materials used. Usually, crash boxes are squared-profiled steel components placed in front of vehicles. Several studies have focused on designing and analyzing new crash boxes with different geometries, materials, and joining techniques to increase their crash mitigation efficiency [3].

Composite materials such as CFRP laminates have been extensively investigated for energy absorption applications, demonstrating their excellent performance and tunability [4-9]. Boria et al. [10] studied the crash-absorbing performance of a CFRP frontal attenuator, demonstrating the effectiveness of using laminated composites for the design of a crash box component. Ozen et al. [11] investigated the crash performance of simple and nested geometries for crash boxes fabricated by laminated CFRP, both experimentally and numerically. They found that the geometry of the external walls of the crash boxes greatly influences the failure patterns and thus energy absorption performances. Also, they observed a specific energy absorption increase for nested geometries. Dominguez et al. [12] investigated the energy-absorbing ability of a crash box designed with a cellular arrangement of pultruded GFRP. They found that this material and its fabrication technique allow for the manufacturing of complicated and efficient structures with excellent specific energy absorption. They also found that the latter decreases with increasing strain rate, passing from a testing speed of $2{\cdot}10^{-4}$ m/s to 4 m/s. Ciampaglia et al. [13] studied the modular design of a CFRP crash

* Corresponding author.
E-mail address: francesco.bandinelli@polito.it (F. Bandinelli).

https://doi.org/10.1016/j.ijimpeng.2025.105401
Received 13 December 2024; Received in revised form 14 March 2025; Accepted 24 May 2025
Available online 24 May 2025

box both experimentally and numerically. They conducted sledge-hammer tests and numerical optimization to reduce mass and increase crash-absorbing efficiency. In recent years more attention has been paid to 3D-printed structures for crash-absorbing purposes because of the design freedom given by 3D printing, both in terms of geometry and properties tailoring. Cellular and lattice structures are examples of the structures that additive manufacturing techniques allow to design, and have been studied for energy absorption purposes [14-16]. Bouteldja et al. [17] investigated the energy absorption performance of 3D-printed polymeric lattice structures via both quasi-static and dynamic compression tests. They found that the polymeric material shows an embrittlement behavior with an increasing strain rate, with consequent strong load drops that limit the specific energy absorption. Andrew et al. [18] investigated the energy absorption characteristics of 3D-printed plate lattices under low-impact loading, analyzing different geometries and orientations of the loading. They found good results in terms of specific energy absorption, also conducting repeated impact tests. Hybrid structures have been investigated to this day, including foam-filled composite structures and foam-filled 3D-printed structures. This helps reduce the weight of crash-absorbing components and improve their specific energy absorption capability. However, until now, a limited number of studies have dealt with the reinforcement of 3D-printed structures with conventional materials. Hou et al. [19] conducted an experimental and numerical study on the design of a crash box fabricated by an internal PA6/CF 3D-printed structure reinforced with an external aluminum shell. The numerical optimization study showed the possibility of tuning the integration between the two components, leading to a reduction of 17 % in weight and an increase of 16 % in SEA compared to a target crash box. Zhou et al. [20] investigated the crash-absorbing potential of a structure produced with a PVC foam reinforced with CFRP tubular pillars. They observed a maximum SEA of 90 kJ/kg and a decrease in performance with increasing strain rate. Sebaey et al. [21] investigated the energy absorption performance of CFRP tubes with different stiffening geometries and foam fillings. They found that the addition of the polymeric foams increases the specific energy absorption and decreases the initial peak load.

To the best of the authors' knowledge, no study has investigated the performance of a CFRP crash box filled with a 3D-printed cellular structure. Most studies that involve these two materials are focused on sandwich panels for blast and perforation purposes [22-25]. The study of hybrid CFRP and 3D-printed crash mitigation components is relevant for the design possibilities offered by the manufacturing process and the consequent tuning and tailoring of the properties. Also, both materials have been previously demonstrated to be relevant in both energy absorption and lightweight purposes.

The present study explores the design and high-speed testing of a composite crash box made by an external CFRP origami-shaped reinforcement and an internal 3D-printed polymeric cellular structure. Origami-shaped structures with two different fillings are 3D printed, and external layers of carbon twill prepreg are applied in different numbers by hand-layup, as schematized in Fig. 1. This allows tuning and balancing between the 3D-printed part and the CFRP reinforcement, analyzing the resultant crash-absorbing potential. Both quasi-static and Split Hopkinson Pressure Bar (SHPB) tests are conducted on the crash boxes, finding interesting results regarding the interaction between the two materials and the performance of the different 3D-printed structures. A finite element model is used to reproduce the dynamic behavior of the tested structures, showing good accuracy in replicating collapse mechanisms and energy absorption. The model is built optimizing the material parameters on a single cellular filling, then its predicting capabilities are proved using it to model the behavior of another cellular filling. The results show good simulation capabilities for the second structure, proving the extendibility of the built model.

2. Materials and methods

In this section, the manufacturing process and the testing setups are described in detail. The crash box geometry comes from previous studies by the authors on the crash-absorbing performance of CFRP front impact attenuators [26,13]. This structure, presented in Fig. 2, aims to exploit the energy-absorption potential of CFRP while avoiding unstable fracture mechanisms such as buckling and sudden failure. The middle plane is in fact characterized by salient and re-entrant angles, providing bending triggers that limit peak loads. Also, this geometrical modification helps promote an extensional behavior of the CFRP reinforcement, which is the most substantial contribution coming from this type of material.

The internal filling part is fabricated by Fused Filament Fabrication (FFF), a common 3D printing technique that allows for the creation of closed-cell structures. From a wide spectrum of possible 3D printing materials, a short carbon-fiber-reinforced PA12 is selected for its high specific mechanical properties. The authors have previously

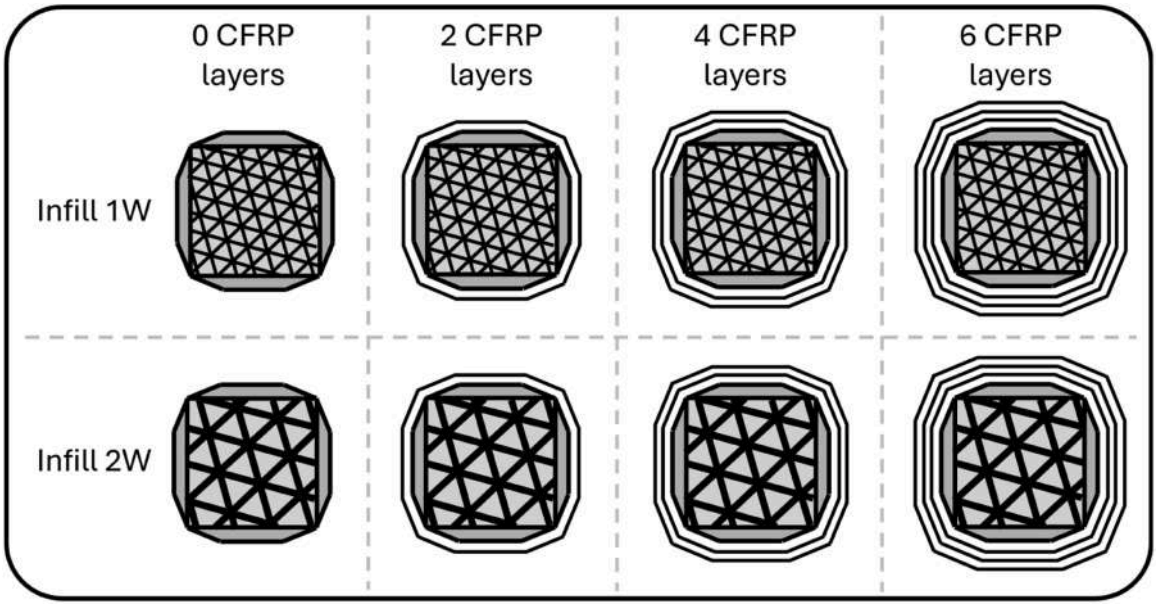

Fig. 1. Scheme of the crash boxes designed. Each contour line represents 2 carbon-epoxy layers.

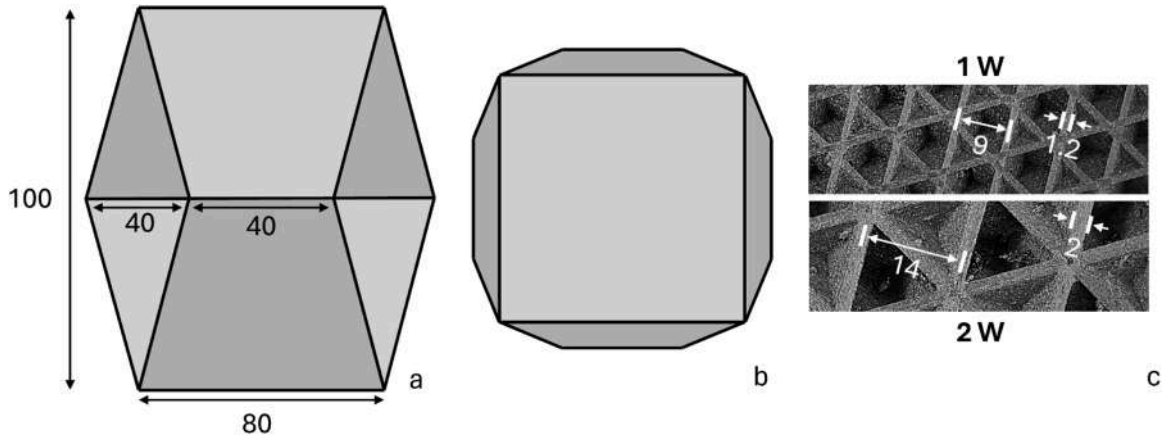

Fig. 2. Scheme of the crash box geometry, with side view (a), top view (b), and details of the internal 3D-printed structures (c). Dimensions are expressed in millimeters.

investigated its mechanical properties in both tension and compression stress states, focusing on its evident anisotropic behavior [27,28]. The FFF intrinsically creates an anisotropic material due to its layered creation process. While anisotropy adds complexity to the understanding of the material, this 3D printing technique allows for the creation of meta-materials and structures that would be impossible with conventional production processes. The internal 3D-printed structure is chosen based on a previous study by the authors on cellular structures used to absorb energy, proving high specific energy absorption [16]. The choice of this plate lattice structure is further motivated by its implementation in existing slicing software, which simplifies the printing process and limits possible printing defects. The selected structure is constituted by a repetition of a closed cubic cell, where the diagonal of the cube is aligned with the vertical printing axis. The cellular structure is intended to mitigate load oscillations during axial compression, partially compensating CFRP fractures. Additionally, the use of an internal polymeric reinforcement provides a die that does not need to be removed afterward, while also limiting the need for CFRP with cost savings. This could be especially true if very low-value polymers are used, such as recycled ones. Recently, several studies focused on the mechanical recycling of thermoplastic materials via 3D printing. Some works showed feasible recycling processes, substantially limiting energy consumption and costs for new components [29-32]. The crash box geometry and details of the infill structure are displayed in Fig. 2. A total of 24 crash boxes are fabricated: 8 for quasi-static tests and 16 for high-speed tests. The 16 crash boxes are identical to the previous 8 but produced in duplicates. Two different infill structures are used, with three different levels of CFRP reinforcement: 2, 4, and 6 layers of carbon twill prepreg (see Fig. 1). One repetition is done for quasi-static tests and two repetitions are done for high-speed tests. The entire experimental campaign is intended to explore different combinations of cellular infill and CFRP reinforcements at two different strain rates. The authors decided to limit the number of repetitions per case while prioritizing an increase in the number of cases. This is motivated by the limited time available for access to the Hoplab laboratory through the "CRUSHAMI" project. Three specimens were prepared for each configuration, and static tests were initially conducted with a single test per case. Since all tests proved effective, the remaining pair of specimens was used for dynamic conditions. Dynamic tests show, in fact, greater complexity and inevitably higher non-uniformity introduced by the dynamic effects in the fracture mechanisms of CFRP.

2.1. 3D printing

The material used for the 3D-printed structures is Nylon Carbon by FiberForce (FiberForce, Treviso, Italy), characterized by a PA12 polymeric matrix reinforced with short carbon fibers (10 wt. %) (Table 1). All crash boxes are printed with an Ultimaker S2+ Connect printer (Ultimaker B.V., Utrecht, Netherlands) using a 0.8 mm diameter Olsson ruby nozzle (3DVerkstan, Stockholm, Sweden). The nozzle printing temperature is set to 260 °C, the printing bed temperature is set to 60 °C, and the cooling fan is switched off. The printing chamber is enclosed and naturally kept at a temperature of about 45 °C by the printing process (bed and nozzle heating), this improves layer adhesion and limits changes in operation temperature during printing.

Two different cellular infill structures are used for the present study, having the same unit cell geometry but different dimensions. These structures are fabricated so that their overall density is kept equal, varying wall thickness and spacing between printed lines. One infill is fabricated with a distance of 9 mm between printed lines and the walls of cells are fabricated by a single pass of the nozzle, and will be referred to as "1W" (Fig. 2). The second infill is produced by increasing the distance to 14 mm between printed lines and using two nozzle passes for the walls of cells, and will be referred to as "2W" (Fig. 2). For the infill 1 W, the thickness of the internal wall is 1.2 mm, while for the infill 2 W, the thickness is increased to 2.0 mm. In both cases the external perimeter of the crash boxes is fabricated by a double pass of the nozzle, to ensure sufficient strength in the interface with the CFRP reinforcement. It is important to highlight that the two infill structures (Figs. 3a and 3b) have the same overall weight (255 g) and density (354 g/l) to compare them using the same amount of material. The infill 1 W is designed to have a more uniform response during compression, while the infill 2 W is designed to explore the possibility of limiting the densification at high strain levels.

2.2. Specimens' fabrication

Carbon twill prepreg is used for the external reinforcement of the 3D-printed parts. Specifically, GG200T-125-E3 125 produced by HP Composite (Ascoli Piceno, Italy) with a fiber volume fraction of 58 % is used. The material is constituted by a balanced twill structure (2 × 2), GG200T, characterized by an areal weight of 200 g/m^2 and a tow size of 3k. Hence, its properties are considered equivalent along the two fiber

Table 1
Summary of the main mechanical properties of Nylon Carbon [32]. "XY" indicates the in-plane directions while "Z" indicates the out-of-plane direction (vertical axis of the printing machine).

XY elastic modulus (MPa)	XY strength (MPa)	Z elastic modulus (MPa)	Z strength (MPa)
1950	46	700	15

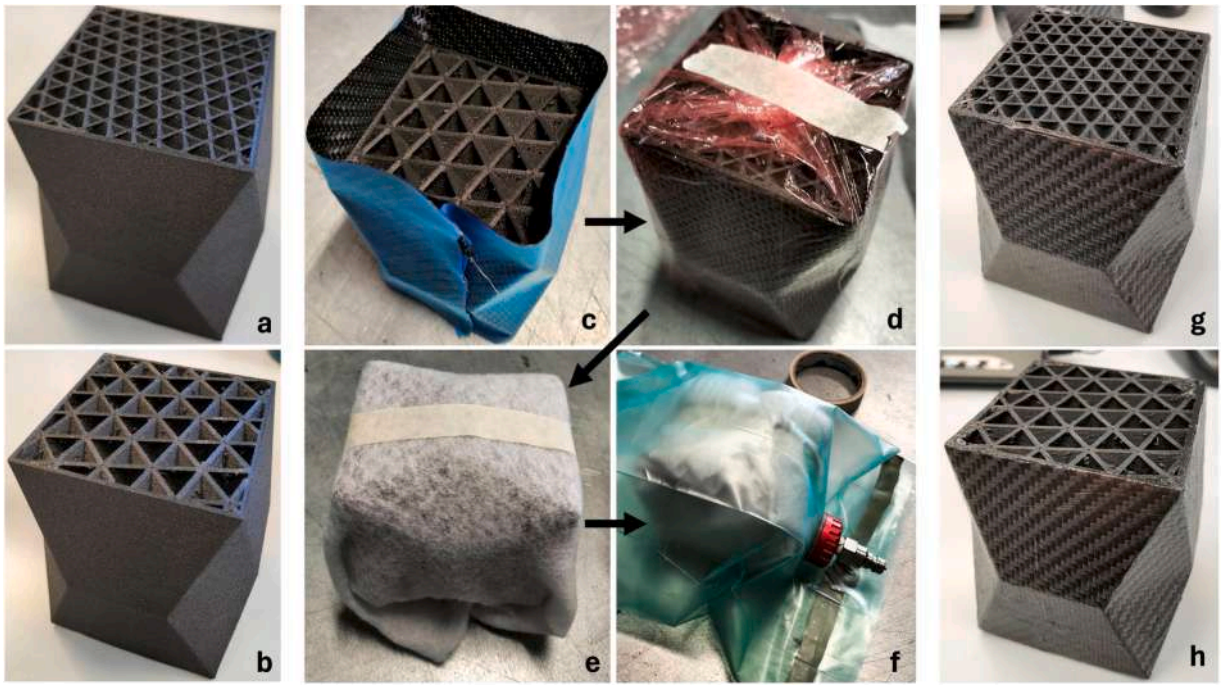

Fig. 3. Images from the hand-layup process. As-printed crash boxes 1 W (a) and 2 W (b). Application of CFRP laminate (c). Peel ply application (d). Breather cloth application (e). Crash box inside a vacuum bag (f). Finished crash boxes (g and h).

directions.

The tensile, shear, and compressive properties of 6-layer CFRP are computed using the ASTM standards D3039, D3518, and D3410, respectively. Tensile and compressive specimens are tested parallel to the fibers' direction (considered equivalent due to the balanced structure), while shear specimens are tested at a 45° angle to the fibers' directions. Results obtained from laboratory tests conducted by the authors are reported in Table 2.

The CFRP reinforcement is draped on the external surface of the 3D-printed parts by hand-layup process and vacuum curing. The surface of the printed parts is cleaned using Loctite SF 7063 degreasing agent (Henkel, Düsseldorf, Germany) and finalized using pressurized air to remove any impurities. As 3D-printed surfaces are characterized by an intrinsic roughness, the surface of the crash boxes is kept as-printed to maximize the interface surface [33,34]. The carbon twill prepreg is cut into large strips able to cover the entire surface of the crash box, representing a single-layer reinforcement, as shown in Fig. 3c. Each layer has an overlap of 10 mm to avoid the gap between prepregs which could trigger premature failures. Once the layup phase is ended, specimens are wrapped in a releasing film which allows for an easy separation once cured (Fig. 3d) and breather cloth (Fig. 3e) to absorb the excess resin and guarantee a uniform pressure under vacuum at −1 bar. A circular sealed vacuum bag is used to put the crash boxes inside an oven for the curing process (Fig. 3f). The latter is constituted by two phases to account for the softening of the 3D-printed part due to high-temperature exposition. The first phase is conducted under vacuum to remove the excess resin, and the temperature is set to 85 °C for 120 min, with a ramp for both heating and cooling. The second phase is conducted at ambient pressure at 125 °C for 60 min, with a ramp for both heating and cooling. In this way, the first curing phase allows to reach sufficient mechanical properties of the CFRP prepreg, while avoiding excessive stress on the 3D-printed part at high temperature and vacuum conditions. Once the component is mechanically stable, the second curing allows it to reach maximum mechanical properties of the CFRP part, while avoiding to stress the 3D-printed part. It is important to highlight that the curing process is also beneficial for the 3D-printed material since it promotes molecular diffusion, hence layer adhesion and better bonding [35,36].

Table 3 presents the average weight of the crash boxes in an as-printed configuration (0 L) and with different numbers of CFRP layers (2 L, 4 L, and 6 L). As can be observed, the printed parts weigh 255 g on average and each carbon-epoxy layer adds an average weight of 12 g The investigated ratios between CFRP reinforcement and 3D-printed infill are 0 %, 9 %, 17 %, and 23 % with 0, 2, 4 and 6 layers respectively. This range of weight ratios allows extending considerations about the design of the crash boxes.

Table 2
Results of the tensile, compressive, and shear tests on CRFP laminate with standard deviations in brackets. For the shear test, the strength limit is given at 5 % of the shear strain.

	Elastic modulus (GPa)	Maximum strength (MPa)
Tension test	63.2 (± 2.3)	687 (± 27)
Compression test	59 (± 1.6)	622 (± 18.5)
Shear test	3.8 (± 0.2)	91 (± 4.1)

2.3. Experimental setup

Quasi-static and high-speed tests are conducted at ELSA (European Laboratory for Structural Assessment) and HopLab facilities at the JRC

Table 3
Mean weights, overall densities, and ratios of the crash boxes in the different manufacturing configurations. The ratio between the CFRP and the 3D-printed part is expressed as the mass fraction of CFRP in the crash box.

Crash box type	Mean total weight (g)	Mean CFRP added weight (g)	Mean overall density (g/l)	CFRP/3D-printed ratios
(1W-2 W) 0L	255	-	354	-
(1W-2 W) 2L	279	24	372	9 %
(1W-2 W) 4L	307	52	398	17 %
(1W-2 W) 6L	329	74	418	23 %

(Joint Research Center) located in Ispra (Italy), in the context of a call for open access to the laboratories, through the project CRUSHAMI. Both quasi-static and high-speed tests are video-recorded for measuring and failure observation purposes. Quasi-static tests are filmed employing a PCO edge 26 camera (Excelitas Technologies, Pittsburgh, United States) with a resolution of 26 MP, at 0.3 fps. The camera is equipped with a Nikon Nikkor 50 mm optical lens (Nikon, Tokyo, Japan). High-speed tests are filmed with a Photron SA5 (Photron, San Diego, United States) at a frame rate of 50′000 fps with a resolution of 448 × 296 px, equipped with a Nikon Nikkor 85 mm optical lens. For both video recordings, a Constellation 120E digital illumination system is used (Veritas, Pasadena, United States). Quasi-static tests are conducted with a servo-hydraulic universal testing machine (ELSA FRANK), with a maximum force capability of 200 kN, at a compression speed of 0.1 mm/s, and a displacement of 70 mm to reach the full densification regime. The engineering strain rate of the quasi-static compression tests is hence 10^{-3} s^{-1}. High-speed tests are conducted on a medium dimension Hopkinson Bar which is schematized in Fig. 4, with a continuous multi-pulse technique [37]. The system is composed of three aluminum (AL7075-T6) bars: a striker bar activated by a pressure tank, an input bar of the same length, and an output bar. The input and output bars are equipped with three strain-gages each, to distinguish propagating waves moving across the bars during the experiment. The striker bar is accelerated to 10 m/s and hits the input bar, compressing the specimen at an initial engineering strain rate of 10^{2} s^{-1}, which is progressively reduced during the test due to the attenuation of subsequent waves [37]. A cardboard is added at the impact location, as a pulse shaper.

Especially with the multi-impulse technique, a proper wave separation method is necessary to distinguish contributions from different waves simultaneously propagating inside the bars. To this end, a deconvolution algorithm is used to identify distinct signals recorded by the six strain-measuring locations [38]. For the calculations, bar properties (density, Young's modulus and Poisson's ratio) are measured from previous tests on a portion of the bar. The frequency dependent wave speed is computed analytically as described in [39,40]. The incident and reflected waves are distinguished to reconstruct the loading history on the specimens in terms of applied displacement and transferred load. Figs. 5a and 5b depict the waves traveling in the input and output bars respectively, showing both signals coming from the strain gages (A, B, and C from the input bar and D, E, and F from the output bar as indicated in Fig. 4) and the reconstructed incoming and outcoming waves at the specimen's interfaces. More specifically, Fig. 5a shows the waves of the input side, while Fig. 5b shows the waves of the output side.

Figs. 5c and 5d depict the displacement and speed histories of the input and output bars during the compression test. As particularly clear in Fig. 5d the multi-impulse of the test affects the speed at which the specimen deforms, with progressively lower speeds as the compression progresses. The resultant displacement has a continuous shape, with no observable oscillation, and optical and strain-gage measurements are in good agreement.

Essentially, the testing system developed behaves, in terms of its effects on the specimen, like a direct impact comparable to a drop-dart test. The main advantage lies in the ability to measure the force and displacement on both sides of the specimen, enabling verification of its balance. Also, the measurements take place without the striker instrumentation, which could be problematic for the sensors' wiring. As shown in Fig. 5d, the specimen remains balanced during the progressive collapse phase, making the test comparable to a quasi-static test in its progression. Having access to both input and output forces eliminates the load cell ringing issues typical of tests with a different setup. The adoption of a multi-impulse system, while making signal processing more complex, significantly reduces the axial dimensions of the apparatus: with the impulse duration achieved using this technique, a Hopkinson bar setup would have required bars over 50 m in length.

3. Results and discussion

3.1. Quasi-static tests

Quasi-static tests are conducted for a single repetition on each specimen type, for a preliminary investigation of the mechanical behavior of crash boxes. Quasi-static tests are important to determine a possible strain rate effect on both the 3D-printed infill and the carbon-epoxy laminate, as already observed in the literature [41,42,12,43]. The results of the quasi-static tests are shown in Fig. 6, as load-displacement curves. For clarity of presentation, the results of the two extreme cases (0 layer and 6 layers) were reported for the two different infill types. Specimens with an intermediate number of layers are proportionally distributed between these two extremes.

Quasi-static curves show increasing mechanical performance with the increasing number of CFRP layers. The addition of external CFRP layers increases the stiffness and the peak load, enhancing the load-bearing capability of the crash boxes (Fig. 6). Progressive damage is experienced by the CFRP external layers with the increase of deformation, hence the gradual reduction of load is evident. The performance enhancement holds until the densification stage, in which total detachment of the carbon layers is reached. At this point, the densification behavior is completely analogous to the unreinforced specimens. The unreinforced crash boxes (1 W and 2 W) are substantially equivalent in terms of mechanical properties, indicating that the quasi-static energy-absorbing behavior is mainly driven by the overall density [44]. The variation of internal structure between the 1 W and the 2 W infills does not translate into a different densification behavior, maintaining a very similar energy-absorbing performance. However, despite having practically identical curves, the two infill structures have different collapse mechanisms. Fig. 7 shows image sequences of the quasi-static tests on unreinforced and 6-layered specimens. Different collapse mechanisms can be observed based on the infill and the reinforcement. The 1 W infill (small cells) has a gradual and symmetric collapse mode, as shown in Fig. 7b The 2 W infill (big cells) is instead characterized by a diffused detachment of the external walls, which drives an asymmetric collapse mode (Figs. 7e and 7f). The mechanical response, seemingly

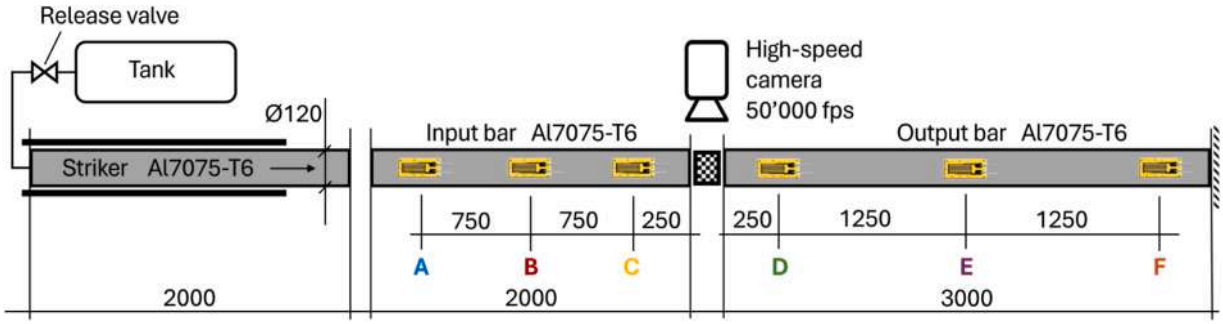

Fig. 4. Scheme of the Hopkinson Bar used for high-speed tests. Dimensions are expressed in millimeters.

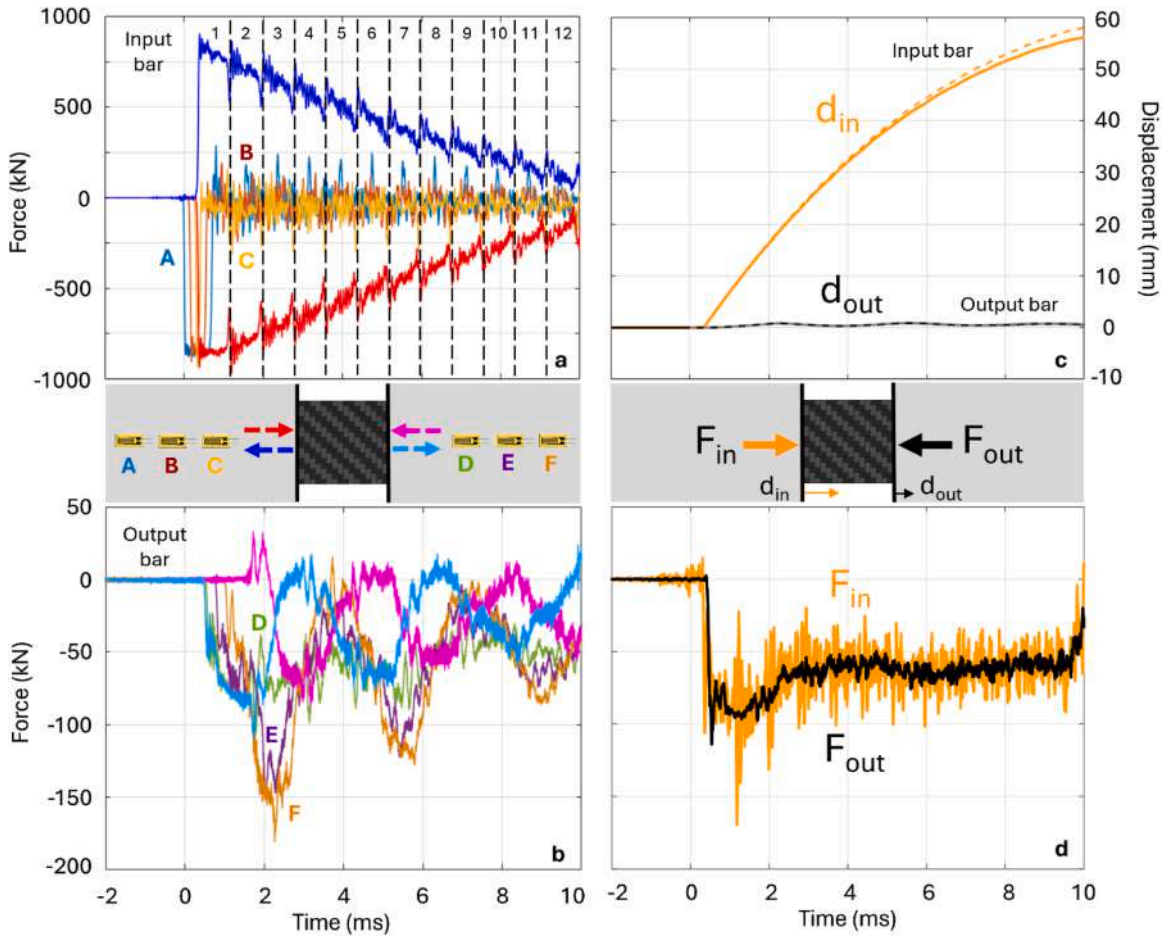

Fig. 5. Traveling waves inside the input (a) and output (b) bars and their reconstructions at the specimen interfaces. Displacement of the input and output bars during the test (c). Signals are distinguished in strain-gage (continuous lines) and optical (dashed lines) measurements. Forces equilibrium check (d).

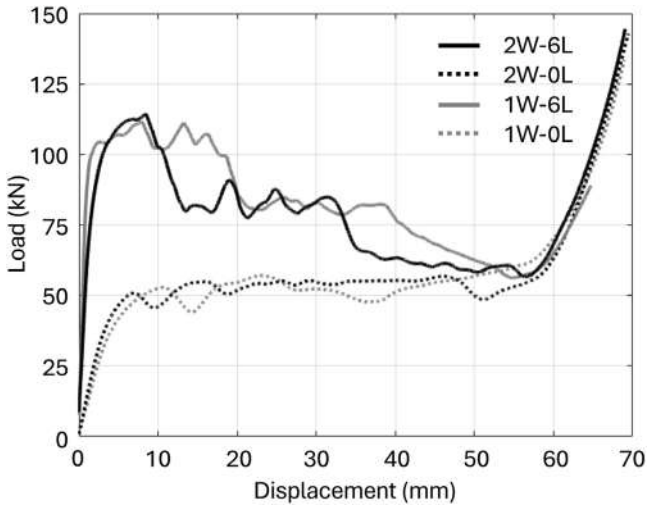

Fig. 6. Quasi-static load-displacement curves.

identical, indicates that the internal parts of the two infill structures behave similarly, while the main difference regards the external 3D-printed walls. This is probably due to the reduced interface between the infill and the external 3D-printed walls, which is observed in the case of bigger cells. The infill structure with fewer cells has fewer and thicker connections to the printed walls, which enhances the localization of stresses and therefore reduces adhesion. Especially with large deformation, as experienced in this type of test, thicker connections are more prone to failure than thinner ones, which can sustain larger deformations without rupturing. This suggests that, besides density, the ratio between the dimensions of the cells and the dimensions of the component is a critical design parameter [45]. Also, a higher number of small cells favors a more uniform distribution of the load across the specimen, thus lowering the stress on the single wall cell. The external CFRP reinforcement triggers the asymmetric collapse mode observed in both 1 W and 2W-filled crash boxes. The early fracture of the top or bottom carbon-epoxy front drives the fracture in the CFRP layers, influencing the collapse behavior.

The interaction between the 3D-printed infill and the external reinforcement is maximum at the beginning of the compression tests, while it is progressively lost with deformation and failure of the adhesive surface. This holds for both infills, even if they have different collapse mechanisms. In the case of the 1 W infill with 6 layers, the uniform and symmetrical deformation of the 3D-printed part effectively reduces the load oscillation that would be present in the case of the sole CFRP layers. The result is a gradual load descent until the start of the densification stage. This is also caused by the outward deformation of some of the cell walls placed on the outside perimeter of the structure. As can be observed in Fig. 7b, the external walls are characterized by prominent ridges caused by the extensive plastic deformation of the 3D-printed material. This progressively reduces the adhesion capability of the CFRP to the 3D-printed part, as a flat surface cannot be consistently ensured. In the case of the 2 W infill with 6 layers, the asymmetrical and more localized collapse mechanism results in a more oscillating behavior, with evident load drops at 10 mm and 35 mm displacement. In

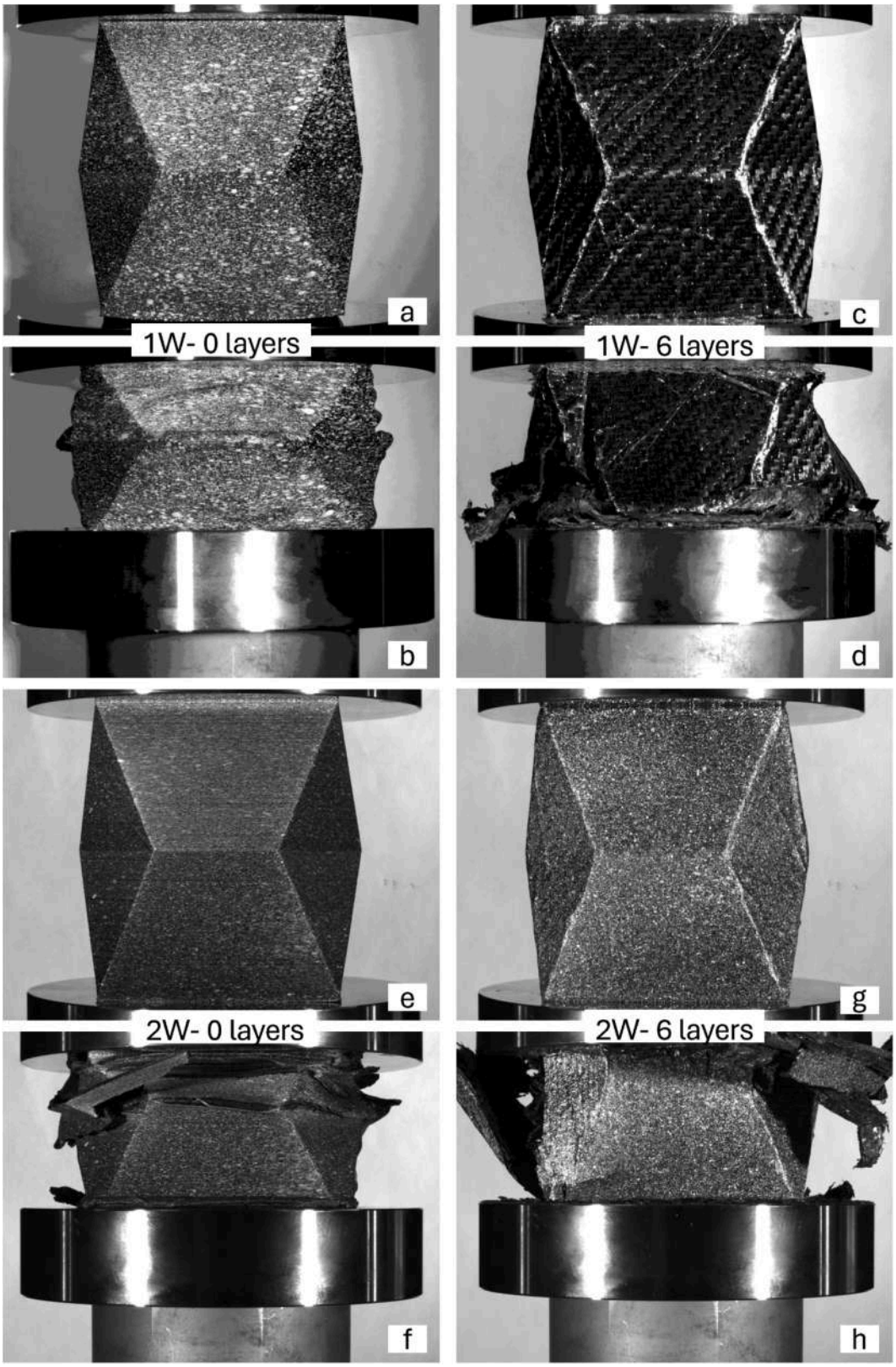

Fig. 7. Image sequences of the quasi-static compression tests conducted on unreinforced and 6-layered reinforced crash boxes (undeformed and collapsed specimens).

this case, the external 3D-printed wall ruptures at multiple locations and causes the CFRP reinforcement to detach from the infill along with it.

Fig. 8 shows the energy absorption performances of the quasi-static tested crash boxes, with specific energy absorption calculated as follows:

$$SEA = \frac{EA}{m} = \int_0^{\delta_f} F d\delta \tag{1}$$

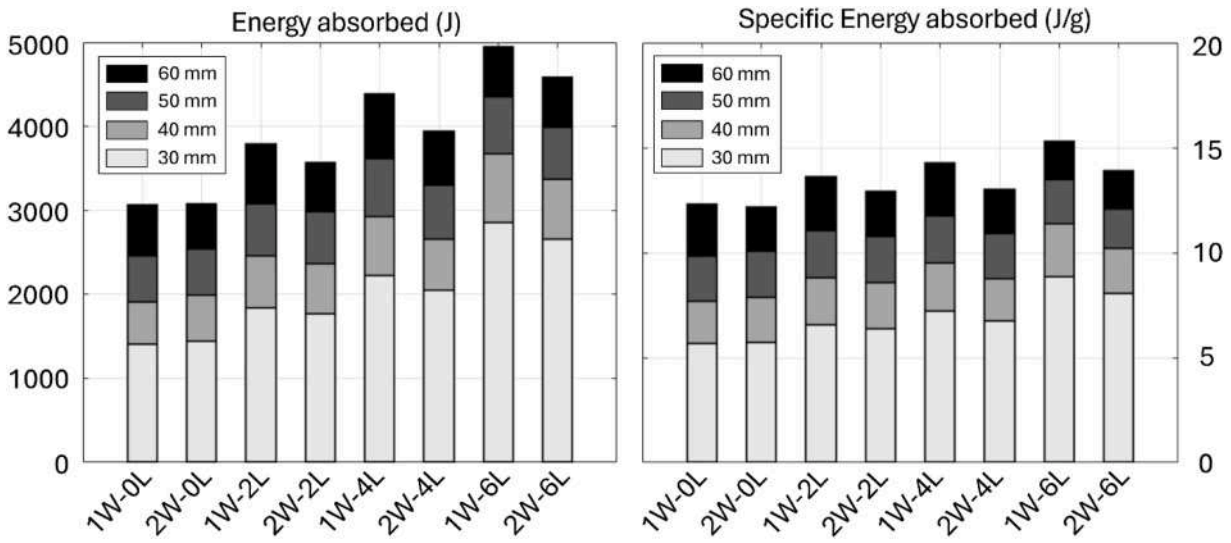

Fig. 8. Graphs of energy absorbed (EA), on the left, and specific energy absorbed (SEA), on the right, for the quasi-static test specimens.

Where m indicates the mass of the specimen and δ_f the crush displacement at the end of the tests. Values are reported until the beginning of the densification stage, observed at a displacement of 60 mm, or equivalently 60 % of engineering strain. Similar values of SEA for the 3D-printed unreinforced structures are found in previous works on cellular structures with similar densities tested at high strain rates [41,46,47]. Compared to conventional solutions, similar values are obtained for steel and aluminum tubes alone (10 and 13 J/g, respectively), while values up to 60 J/g are obtained for CFRP tubes [48]. Aluminum extruded crash boxes with square sections have been proven to have specific energy absorptions in the range of 10–20 J/g [49]. The energy absorption gradually increases with the addition of external CFRP layers, as expected. Interestingly, the specific energy absorption (SEA)

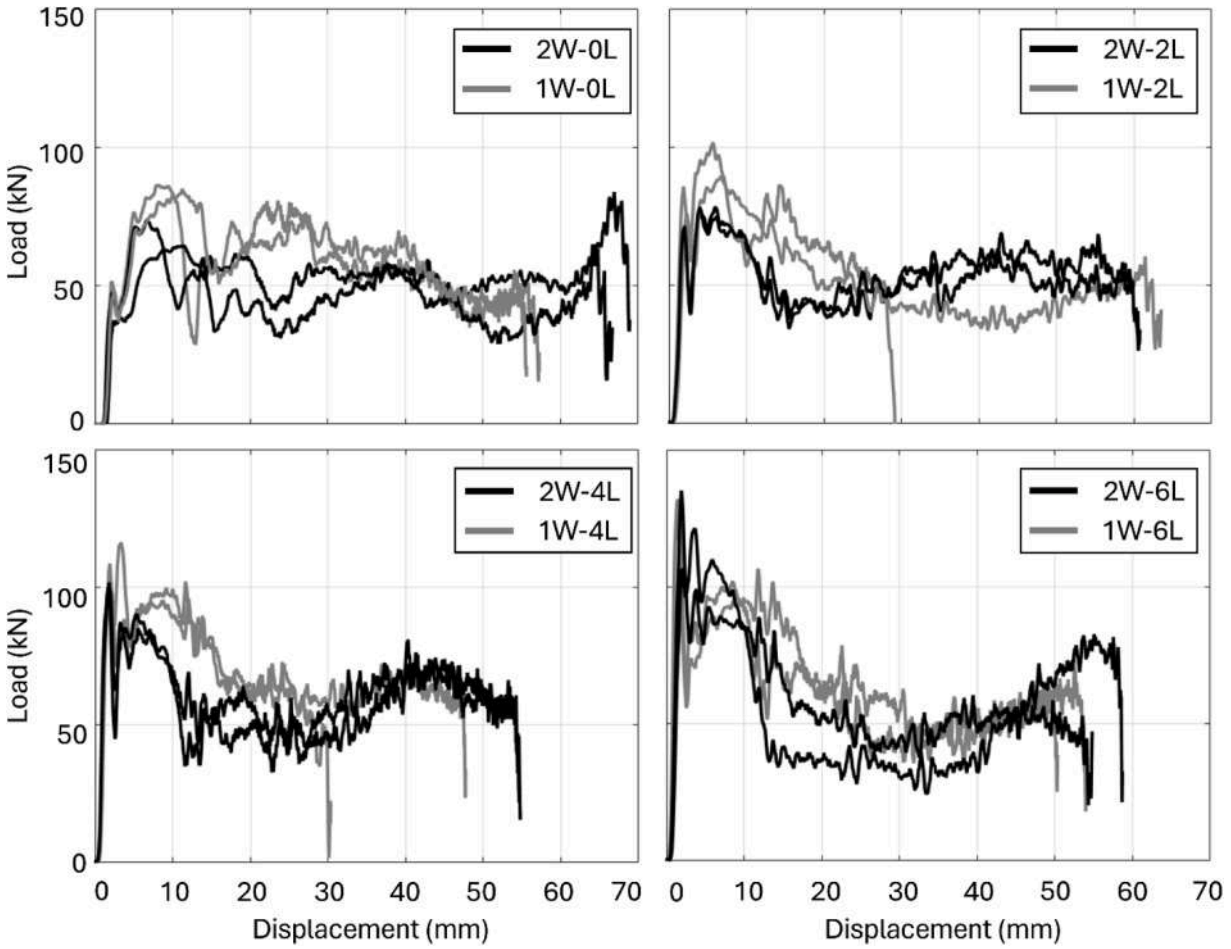

Fig. 9. Load-displacement curves of the SHPB tests conducted on unreinforced (0 L) and reinforced (2 L, 4 L, and 6 L) crash boxes.

increases as well, demonstrating that the addition of CFRP layers is beneficial for the efficiency of the components, other than their absolute performance. The 1 W cellular structure, which is characterized by smaller cells, demonstrates higher specific energy absorption for all the tested conditions, proving its better suitability for energy-absorbing purposes.

3.2. High strain rate tests

Fig. 9 shows the load-displacement curves of the SHPB tests. As already observed in the quasi-static tests, the addition of external CFRP layers enhances the peak loads and the initial stiffness of the crash boxes. Interestingly, the maximum peak load of the unreinforced 1 W crash boxes shifts from 53 kN to 86 kN, while the same enhancement does not occur for the 2 W structure. This indicates that the polymeric material experiences a strain rate-driven stress enhancement [50-52], but it also suggests a strong variation in the high strain rate behavior based on the cell geometry. In fact, in the same testing conditions, the peak load of the 2 W unreinforced crash boxes rises from 51 kN to 64 kN only. Again, this is due to the weaker connection of the infill to the 3D-printed walls, which is worsened by the embrittlement of the polymeric matrix at higher strain rates [53].

As already observed, the 2 W infill is in fact more prone to sudden failures, which is even more evident at higher strain rates, as shown in Fig. 11. Unlike the quasi-static tests, the load drops associated with failure are generally more pronounced, especially in the case of reinforced crash boxes. As an example, the gradual descent of load to 50 kN experienced by the 6-layered structure is observed to happen in the first 30 mm of compression. The same happens during the first 50 mm of compression in the quasi-static tests. For 2-layered and 4-layered crash boxes, analogous considerations can be made.

Fig. 10 shows the results of the SHPB tests in terms of energy absorption and specific energy absorption. The missing values of the 1W-4 L crash boxes at 50 mm are due to the test not reaching the desired displacement. As observed in the load-displacement curves, the dynamic mechanical performance of the CFRP-reinforced crash boxes is lower than the quasi-static one. Energy absorption and specific energy absorption confirm this observation. Comparing the latter quantities at 50 mm of displacement (50 % of engineering deformation), notable differences can be observed. Table 4 summarizes the relative differences in terms of specific energy absorption and crush force efficiency (CFE) between the quasi-static and dynamic testing conditions. None of the 1W-4 L specimens reached 50 mm; therefore, their estimated values are extended based on the projection of the curves and reported in Table 4 in italics format.

The CFE is calculated as follows:

$$CFE = \frac{Fmean}{Fpeak} \tag{2}$$

Where F_{peak} indicates the maximum initial peak load and F_{mean} indicates the mean force after F_{peak} is reached.

Except for the 1 W unreinforced crash box, the specific energy absorption decreases when passing from the quasi-static regime to the high strain rate one. The crush force efficiency decreases as well, with progressively increasing differences as the number of CFRP layers increases. This is also caused by high initial load peaks, which are inevitably higher in SHPB tests due to inertia effects and the materials' strain rate sensitivity. This behavior change is mainly due to two reasons: the change in the collapse mechanism of the 3D-printed infill and the embrittlement of the epoxy matrix. The latter also affects the interface strength between the printed part and the CFRP reinforcement. The change in the collapse mode of 3D-printed polymeric structures due to the high strain rate has been already observed in past works [46,54,55]. Besides the strain rate effect on the polymer matrix, a possible explanation for the remarkable 20 % enhancement in SEA obtained for the 1 W unreinforced crash box is the secondary effect of entrapped air. As already studied in past works with comparable testing strain rates [56-58], cellular structures show a crushing stress enhancement due to the effect of entrapped air. This effect has also been linked to a change in the bending behavior of the cell walls in cellular structure [58]. The trapped air could be responsible for the structure's outward collapse, affecting the crush behavior. This is particularly observable in the case of the 1 W infill structure, shifting from the quasi-static to the dynamic regime. The collapse mode of the quasi-static test is characterized by a homogeneous deformation with both inward and outward-going cell walls. In the dynamic regime, the collapse mode is instead characterized by only outward movements of the whole structure. Also, this mechanism is responsible for the worsening of the adhesion with the external CFRP walls, which explains the abrupt detachments observable in the dynamic tests of reinforced crash boxes (Figs. 11 and 12). The effect of entrapped air is not evident in the 2 W infill structure because of the rupturing experienced from the first phases of the compression tests. Also, a structure with bigger cells is more prone to lose air-tightening, even with less diffused failures.

Regarding the effect of the strain rate on the CFRP external walls, the embrittlement of the epoxy matrix is responsible for the change in the failure modes. As observed in [59], with the increase in strain rate, the

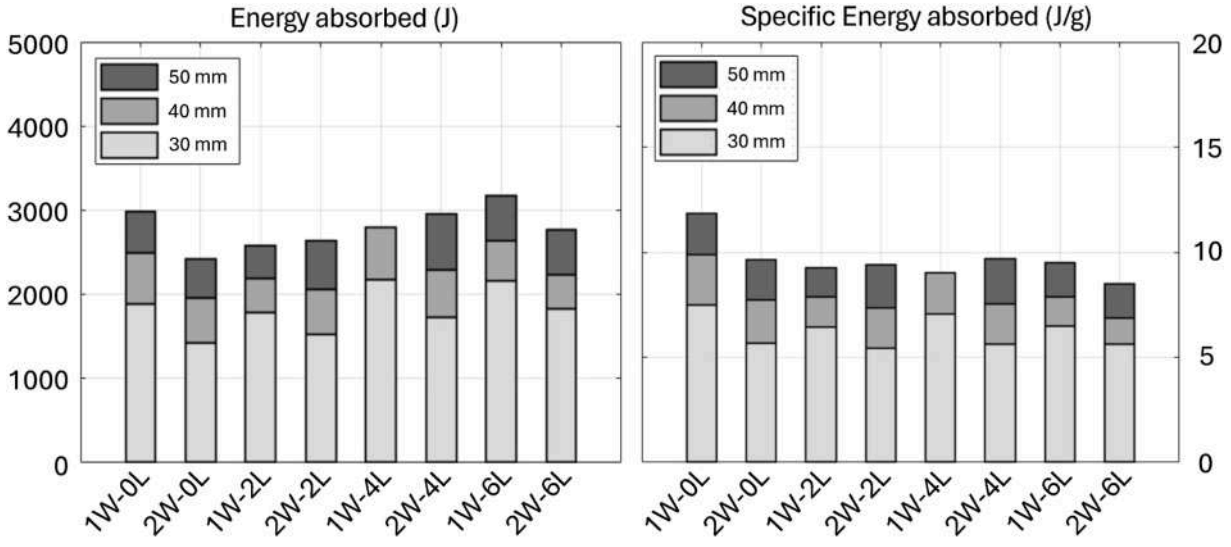

Fig. 10. Graphs of energy absorbed (EA) on the left, and specific energy absorbed (SEA) on the right, for the SHPB test specimens.

Table 4
Summary of the differences between quasi-static and dynamic SEA and CFE evaluated at 50 mm of displacement. Italics formatted values are estimated because the test did not reach 50 mm displacement.

Specimen	Quasi-static SEA (J/g)	Dynamic SEA (J/g)	Difference (%)	Quasi-static CFE (%)	Dynamic CFE (%)	Difference (%)
1W-0L	9.86	11.84	+20.1	98.7	67.6	−31.5
2W-0L	10.07	9.62	−4.5	99.6	71.5	−28.2
1W-2L	11.04	9.25	−16.2	87.4	53.9	−38.3
2W-2L	11.26	9.42	−16.3	92.5	68.2	−26.3
1W-4L	12.05	*10.55*	*−12.5*	79.6	*64.2*	*−19.4*
2W-4L	11.88	9.71	−18.3	78.4	57.8	−26.3
1W-6L	13.49	9.49	−29.7	76.1	43.7	−42.6
2W-6L	12.07	8.52	−29.4	66.8	41.3	−38.2

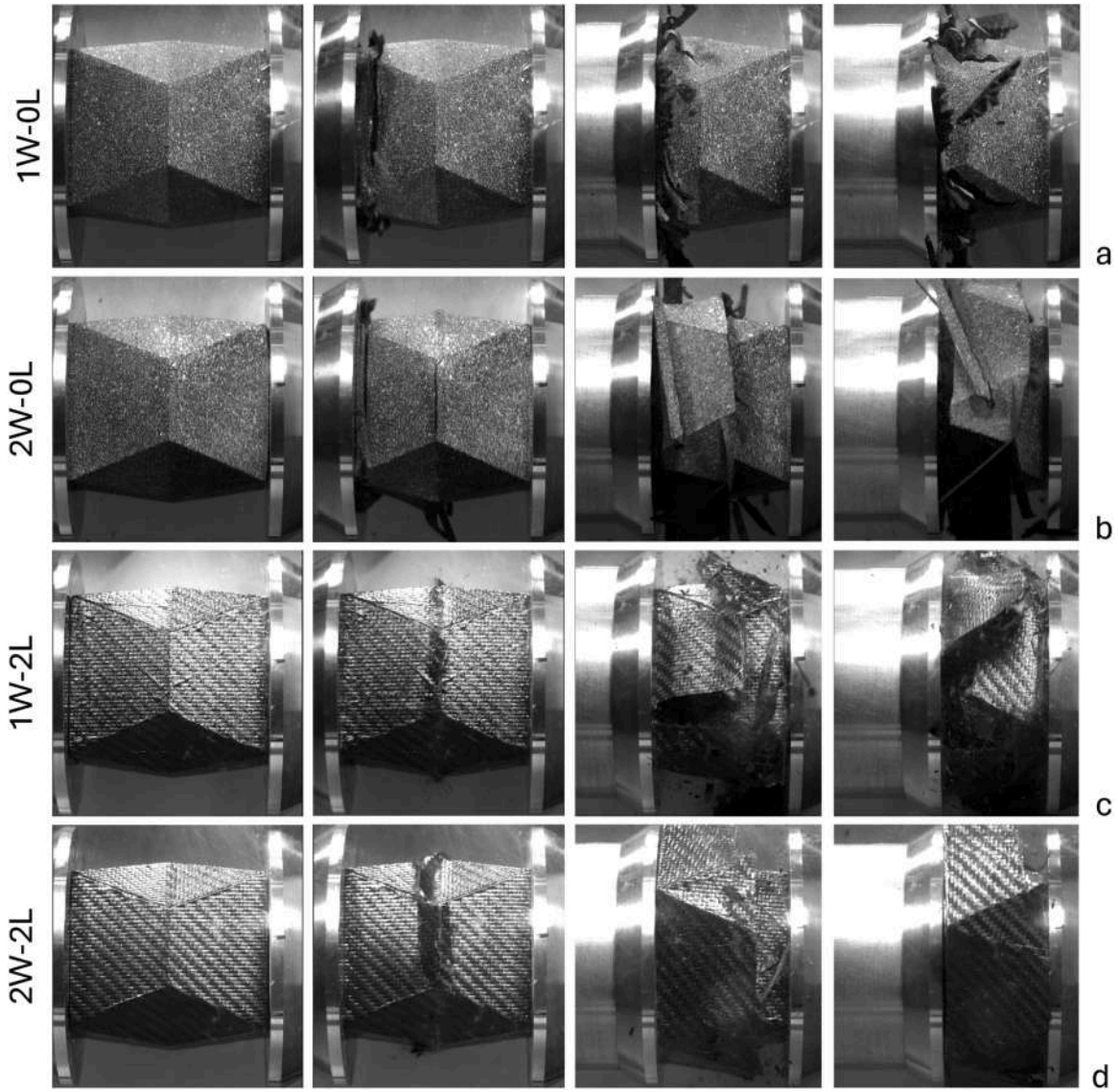

Fig. 11. Image sequences of the SHPB tests on 1 W unreinforced (a), 2 W unreinforced (b), 1 W reinforced with 2 layers (c), and 2 W reinforced with 2 layers (d).

ultimate compressive strain of a carbon-epoxy laminate reduces sensibly. Also, the failure mode shifts from progressive delamination observed in quasi-static tests to a sudden failure across plies in the high strain rate tests. This could explain the failure mechanism observed in the SHPB tests, with the CFRP reinforcement failing suddenly in the middle plane of the structure. Also, little to no delamination is observed, confirming previous observations. A similar decrease in specific energy absorption of CFRP structures under high strain rate compression has been observed in past studies [12,43,60]. Section 3.3 discusses the observed failure modes.

3.3. Failure analysis of SHPB tests

As observed in past works about the crashworthiness of FRP composites, the energy absorption performance of these materials is negatively affected by strain rate. This aspect is often underexplored and needs to be addressed to promote the proper design of FRP structures for crash-absorbing purposes. Dominguez et al. [12] observed a radical

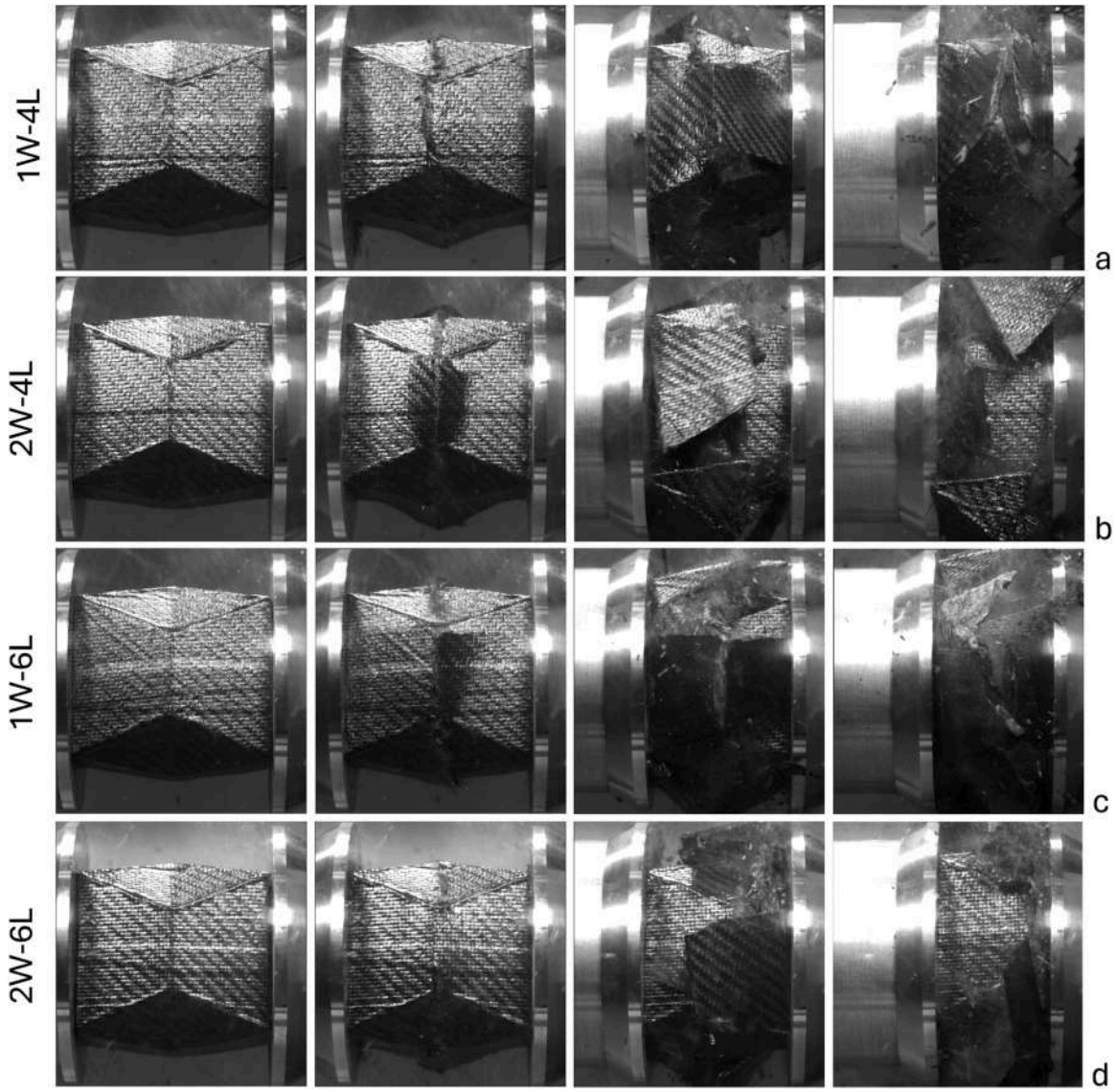

Fig. 12. Image sequences of the SHPB tests on 1 W reinforced with 4 layers (a), 2 W reinforced with 4 layers (b), 1 W reinforced with 6 layers (c), and 2 W reinforced with 6 layers (d).

change in the collapse mechanism of the designed crash box when passing from quasi-static tests (10 mm/min) to dynamic ones (15 km/h). While a progressive failure mechanism (with very limited load oscillations) was observed in the quasi-static tests, a more unstable and sudden rupture was observed in dynamic ones. Fu et al. [60] noted a decrease in energy absorption performance and a change in the fracture mechanisms of their CFRP foam-filled crash-absorbing component when shifting from quasi-static to dynamic loading. They experienced extended tensile failures when the structure was subjected to quasi-static loading, while shear-driven failures were observed in the dynamic regime. Studies that report a decrease in the energy absorption performance of FRP components due to strain rate, usually attribute this effect to the change in failure mechanisms with increasing testing velocity.

In the present study, a substantial change in failure and collapse mechanism is observed passing from the quasi-static to the dynamic loading of the crash boxes. Hence, a discussion on the observed behavior is presented to highlight the need to understand and address these issues.

Fig. 11 depicts image sequences of the SHPB tests, showing the fracture behavior of the unreinforced (10a and 10b) and 2-layered reinforced crash boxes (10c and 10 d). The 1 W unreinforced crash box (11a) changes its behavior from a uniform collapse observed in the quasi-static tests to a localized fracture mechanism propagating along the axial direction. Also, while in quasi-static tests no evident fracture is observed, impact tests show diffused detachment of external walls with portions of the infill structure. The 2 W unreinforced crash box (11b) in dynamic testing conditions shows a similar behavior to the one observed in the quasi-static tests. However, the fracture surfaces involve larger portions of the infill part besides external walls. In quasi-static tests, the fracture behavior of the reinforced crash boxes is mainly triggered by the face in contact with the testing machine, where imperfections are easier to be found. In SHPB tests, the reinforced crash boxes' triggering mechanism is the fracturing of the CFRP walls in the middle plane. At this location, the angular difference between the CFRP faces is maximum, therefore the walls are critically stressed in bending mode. The resulting collapse mechanism is an interpenetration of the two CFRP halves, considered an unstable propagation mode. This fracture behavior is responsible for the evident load drops visible in the initial phase of the load-displacement curves of reinforced crash boxes (Fig. 9).

Fig. 12 shows image sequences of the SHPB tests on 4-layered and 6-layered crash boxes. After the initial interpenetration of the two CFRP halves, the fracture pattern favors a rapid detachment of the CFRP walls

from the internal 3D-printed part. In most cases, the reinforcement is completely detached before the end of the test (as clearly visible in Fig. 12b), leaving the 3D-printed component solely tasked with load-bearing and energy-absorption actions. This explains the great reduction of SEA from the quasi-static to the dynamic testing regime (Table 4). Unfortunately, large portions of the external CFRP are detached without notable deformation, which implies that the energy absorbed by those portions is virtually none. The results highlight the need for improvement in the design of a hybrid structure for high-speed impacts: enhancement of the adhesion interface to maintain interaction between the two materials; improvement of the component shape to better exploit the CFRP performance; and improvement of the balancing between the 3D-printed infill and the CFRP walls. Promising results are obtained in the case of the quasi-static tests, showing that joining 3D-printed parts with carbon-epoxy composites is suitable. High strain rate tests show that a more appropriate design procedure should be followed to make these components suitable for impact scenarios, as their behavior is greatly affected by strain rate.

4. Finite element model

An explicit finite element model is proposed to reproduce the high strain rate behavior of the crash boxes. The model is built in LS-Dyna environment, replicating the geometry of the 3D-printed part, using shell elements for both the 3D-printed part and the CFRP reinforcement. Exploiting the symmetry of the crash box, only a quarter of the entire crash box is modeled, as shown in Fig. 13.

4.1. Model definition

The finite element model is built taking the 1 W unreinforced crash box as a reference. The model is meshed with fully integrated shell elements with an average dimension of 2 mm. The nodes of the boundary of the quarter model are fixed to slide in the symmetrical planes only. Two rigid walls are used to impose a compression of 60 mm in 10 ms, similarly to the experimental tests. The material model used for the 3D-printed infill is an elasto-plastic isotropic material with kinematic hardening (MAT_PLASTIC_KINEMATIC). The choice of an isotropic material is motivated by the will to propose a simplified modeling strategy, avoiding the anisotropic modeling that the 3D-printed material would generally need. In addition, the crash boxes are constituted by a peculiar cellular structure and are subjected to a specific loading condition, factors which possibly limit the effects of anisotropy. Different orientations of the printed material (inclined walls) and a loading condition that mainly stresses the material inside the horizontal plane (as testified by the outward fracture mechanisms) mitigate the strong anisotropy that characterizes it. The material parameters are optimized starting from the experimental evidence of previous work by the authors [32], modified iteratively to account for strain rate effects on the polymeric material. The density is adjusted from the nominal value (1 g/mm^3) to match the exact weight of the crash boxes: as observed in the previous work, the 3D-printed material is characterized by a very high fraction of void [32]. The final parameters are indicated in Table 5.

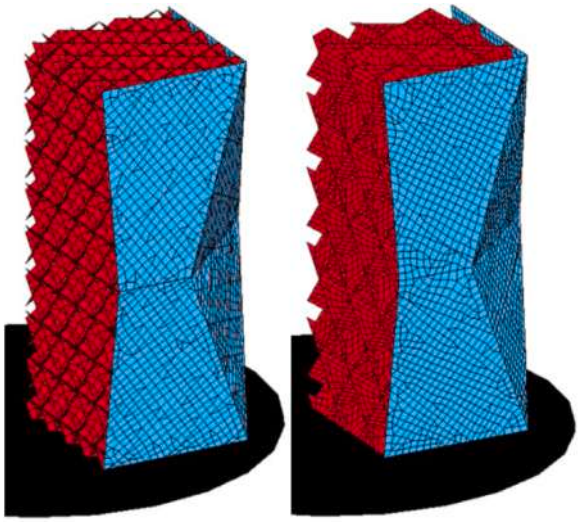

Fig. 13. FEM model for 1 W (left image) and 2 W (right image) crash boxes.

A failure criterion is implemented to model the fracture behavior of the 3D-printed material. MAT_ADD_EROSION is used, combining a maximum principal stress limit of 65 MPa and a maximum equivalent plastic strain of 0.08. The external CFPR reinforcement is modeled by fully integrated shells with the same average mesh dimension, replicating the mesh of the external 3D-printed wall. The material model used is MAT_ENHANCED_COMPOSITE_DAMAGE, which is derived from the experimental tests conducted on the CFRP laminate, as described in Section 2.2. The material's parameters used in the model are presented in Table 6.

The balanced twill prepreg is modeled by giving the same properties to the two directions a and b in the laminate plane. In the table, $\sigma_{i,c}$ is the compressive stress limit of the i th direction, while $\sigma_{i,t}$ represents the tensile stress limit. The shear stress limit is defined as τ_{ab}, while the tensile and compressive fiber failure strains are defined as $\varepsilon_{f,t}$ and $\varepsilon_{f,c}$ respectively. The values of Young's modulus are assumed to be the average value between the tensile and compression values. The bond between the CRFP shell and the 3D-printed wall is modeled by a tiebreak contact (TIEBREAK_SURFACE_TO_SURFACE) with normal and shear stress limits of 16 MPa and 12 MPa, respectively. The stress limits are found by iteratively changing the values, verifying detachment, and comparing the collapse modes with the experimental tests on the crash boxes.

4.2. Results

The results of the finite element models are presented with the experimental load-displacement and energy-displacement curves, as shown in Figs. 14 and 15. The green shell represents the carbon layers, the blue shell represents the external wall of the 3D-printed structure, and the red part represents the internal 3D-printed infill. The accuracy of the finite element model is particularly evident for the case of the 1 W unreinforced crash box, which is the case study used to tune the parameters of the 3D-printed material. The models satisfactorily represent the reinforced structures, as the overall behavior is generally captured, and the absorbed energies are close to the experimental values. For the 1 W geometry, the maximum relative error in terms of energy absorbed is 10.5 % for the 1 W 2 L crash box, while the maximum error in terms of peak load is 36 % for the 1 W 6 L crash box. As observed in the experimental tests, the addition of the CFRP layers triggers a different collapse mechanism, which is captured by the finite element models. The numerical model is able to capture the effect of the reinforcement: the addition of carbon layers enhances the peak load of the structures, which is then quickly reduced by an initial sudden failure. Also, the addition of more layers facilitates the detachment of big portions of CFRP, as observed in the experimental tests. The model, tuned for the 1 W infill, satisfactorily represents also the energy absorption behavior of the 2 W infill, while it is slightly less precise in the modeling of the failure behavior of the crash boxes. The carbon layers detach together with the external 3D-printed walls (Fig. 15), which means that portions of 3D-printed walls are removed from the structure as only partially

Table 5
Material parameters for the 3D-printed part.

ρ (g/mm^3)	E (MPa)	ν (-)	σ_y (MPa)	E_{tan} (MPa)
$8{\cdot}10^{-4}$	1300	0.2	45	60

Table 6
Material parameters for the CFRP part. Letters a and b refer to the material's directions in the laminate plane.

ρ (g/mm^3)	E_a (MPa)	E_b (MPa)	ν (-)	G_{ab} (MPa)	G_{bc} (MPa)	G_{ca} (MPa)
0.0145	61,000	61,000	0.083	3800	3800	3800
$\sigma_{a,c}$ (MPa)	$\sigma_{a,t}$ (MPa)	$\sigma_{b,c}$ (MPa)	$\sigma_{b,t}$ (MPa)	τ_{ab} (MPa)	$\varepsilon_{f,t}$ (-)	$\varepsilon_{f,c}$ (-)
622	687	622	687	91	0.005	−0.01

observed in the experimental tests. However, this effect only drags away a minor contribution in term of energy absorption, since the carbon layers are expected to detach anyway and the 3D-printed external wall is only a minor portion of the structure. This is also confirmed by the load-displacement and energy-displacement curves, which reflect a good approximation of the overall behavior. Compared to the 1 W structures simulation, the only change is the geometry of the infill, indicating that it is the main responsible for the mismatch between the experimental and the numerical collapse dynamics. For the 2 W geometry, the maximum relative error in terms of energy absorbed is 10.7 % in the early stages of compression of the 2 W 4 L crash box, while the maximum relative error for the peak load is 39 % for the 2 W 6 L crash box. While still providing useful indications about the overall behavior, the load-displacement curves of the 2 W FEM models show less capability of capturing the same load oscillations observed in the experimental tests. Generally, the outward projection of debris observed in the experimental tests is instead limited in the finite element simulations. This could be an indication that the effect of entrapped air (which is not considered in the models) can partially contribute to the early fracturing of the 3D-printed parts.

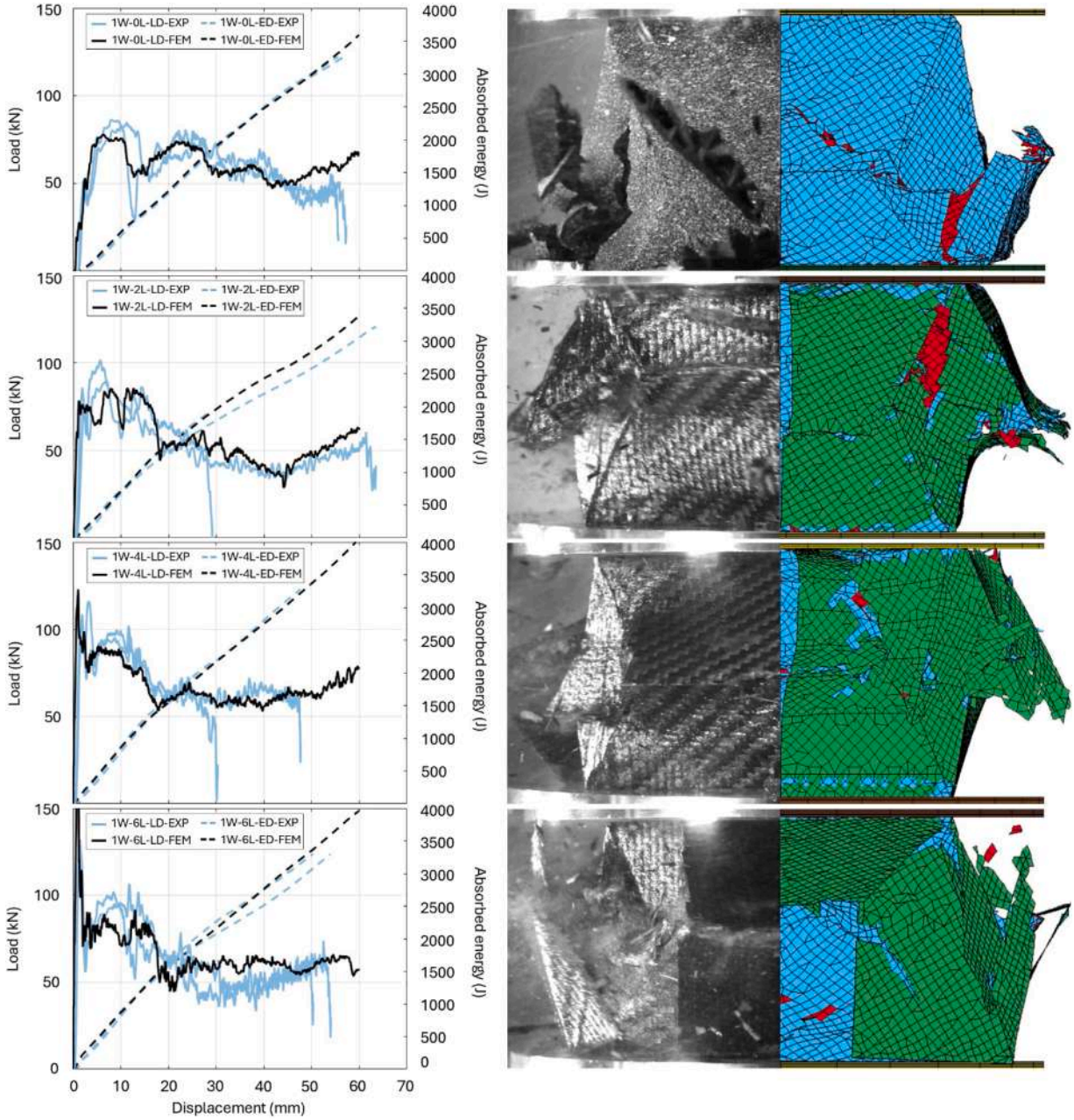

Fig. 14. Comparison of experimental (blue) and numerical (black) curves for 1 W infill crash boxes. Continuous lines represent load-displacement curves (LD) while dashed curves represent energy-displacement curves (ED).

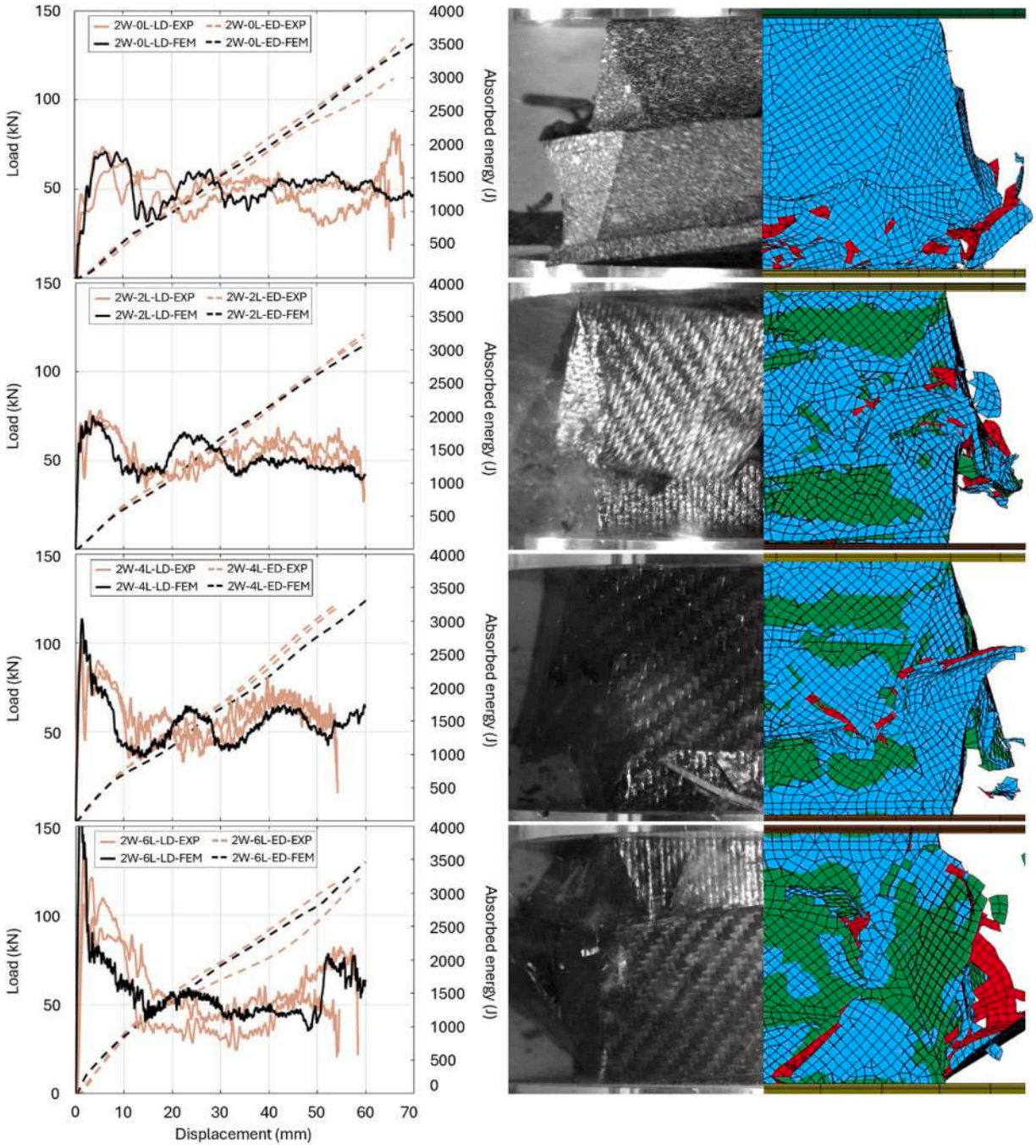

Fig. 15. Comparison of experimental (orange) and numerical (black) curves for 2 W infill crash boxes. Continuous lines represent load-displacement curves (LD) while dashed curves represent energy-displacement curves (ED).

5. Conclusions

In this study, quasi-static and high strain rate tests are conducted on hybrid 3D-printed and CFRP structures for crash-absorbing applications. Specimens with two different 3D-printed cellular structures and different ratios of CFRP and 3D-printed parts are produced by FFF and hand-layup technique. High strain rate tests are conducted on a split Hopkinson pressure bar with a multi-impulse technique to produce sufficient compressive displacement. A finite element model is proposed to mimic the collapse dynamics of the structures and replicate their energy absorption behavior. The 3D-printed material's model is tuned based on the results of the 1 W unreinforced crash box and it is not modified when simulating the other structures and infill type to explore its extensibility.

Quasi-static tests show that adding CFRP external walls enhances the energy absorption capability of the crash boxes, with increasing specific energy absorption over 15 J/g. Carbon-epoxy laminate increases the stiffness of the structure and implies a higher plateau stress. The collapse behavior of crash boxes is significantly influenced by the infill structure, which can consist of smaller or larger cells. For a given overall density, structures with smaller cells are more effective as they exhibit a gradual and uniform collapse mechanism. Additionally, smaller cells provide a more consistent interface between the 3D-printed infill and the walls, resulting in stronger bonding and enhanced structural integrity.

High strain rate tests show notable differences compared to the quasi-static tests. Even if the 3D-printed structures show a specific

energy absorption increase of up to 20 % with a rising strain rate, all other crash boxes show a substantial decrease in crash-absorbing performances. The SEA and CFE are greatly reduced, especially for highly reinforced crash boxes (such as 6-layered ones), with maximum reductions of around 30 % and 40 %, respectively. The main reason for this evident drop in performance is explained by the different failure modes observed during the tests. During high strain rate tests, in the first stages of compression, a sudden failure of the middle plane of the structures triggers the rapid detachment of the external CFRP walls. This is reasonably due to the embrittlement of the epoxy matrix in the impact scenario and a triggering mechanism represented by the angular change in the orientation of the CFRP walls at the middle plane. Also, past works dealt with the effects of entrapped air in closed-cell structures, showing that besides enhancing the energy-absorption performance, it also usually implies a change in the collapse behavior. Specifically, the entrapped air could be responsible for the outward expansion of the cellular structure during compression, which penalizes the adhesion at the interface with the CFRP reinforcement. The finite element model here proposed is able to capture the behavior of the crash boxes, also proving to be extensible to a different cellular structure. The model shows a good approximation in both the simulation of the collapse dynamics and the energy-absorbing behavior, and it can be considered useful for preliminary design purposes.

Proper modifications of the adhesion interface and component shape could allow for better exploitation of the interesting mechanical and energy-absorption characteristics of these structures, as shown by the quasi-static tests. A different design method should be followed for high strain rate applications. Different failure-triggering methods and bonding strategies should be addressed in future work to contrast the negative effects of the impact loading on hybrid 3D-printed and CFRP-reinforced crash boxes.

Author's statement

All authors have agreed to the published version of the manuscript.

CRediT authorship contribution statement

Francesco Bandinelli: Writing – review & editing, Writing – original draft, Visualization, Software, Methodology, Investigation, Formal analysis, Data curation, Conceptualization. **Alberto Ciampaglia:** Writing – review & editing, Validation, Methodology, Investigation, Formal analysis, Data curation, Conceptualization. **Raffaele Ciardiello:** Writing – review & editing, Validation, Supervision, Resources, Methodology, Investigation, Formal analysis, Data curation, Conceptualization. **Lorenzo Peroni:** Writing – review & editing, Visualization, Validation, Supervision, Resources, Project administration, Methodology, Investigation, Funding acquisition, Formal analysis, Conceptualization. **Marco Peroni:** Writing – review & editing, Validation, Supervision, Software, Resources, Methodology, Funding acquisition, Formal analysis, Data curation. **Martina Scapin:** Writing – review & editing, Visualization, Validation, Supervision, Resources, Project administration, Methodology, Investigation, Formal analysis, Conceptualization.

Declaration of competing interest

The authors declare that they have no known competing financial interests or personal relationships that could have appeared to influence the work reported in this paper.

Acknowledgments

The experimental data used in this research were generated through access to the ELSA HopLab under the Framework of access to the Joint Research Centre Physical Research Infrastructures of the European Commission (CRUSHAMI project, Research Infrastructure Access Agreement Nr. 537 36692-1/2022-1-RD-ELSA-HopLab).

Data availability

Data will be made available on request.

References

[1] Sun G, Chen D, Zhu G, Li Q. Lightweight hybrid materials and structures for energy absorption: a state-of-the-art review and outlook. Thin-Walled Struct 2022;172 (November 2021):108760. https://doi.org/10.1016/j.tws.2021.108760.
[2] Obradovic J, Boria S, Belingardi G. Lightweight design and crash analysis of composite frontal impact energy absorbing structures. Compos Struct 2012;94(2): 423–30. https://doi.org/10.1016/j.compstruct.2011.08.005.
[3] Peroni L, Avalle M, Peroni M. The mechanical behaviour of aluminium foam structures in different loading conditions. Int J Impact Eng 2008;35(7):644–58. https://doi.org/10.1016/j.ijimpeng.2007.02.007.
[4] Reuter C, Sauerland KH, Tröster T. Experimental and numerical crushing analysis of circular CFRP tubes under axial impact loading. Compos Struct 2017;174:33–44. https://doi.org/10.1016/j.compstruct.2017.04.052.
[5] Sun G, Li S, Li G, Li Q. On crashing behaviors of aluminium/CFRP tubes subjected to axial and oblique loading: an experimental study. Compos B Eng 2018;145 (March):47–56. https://doi.org/10.1016/j.compositesb.2018.02.001.
[6] Isaac CW, Ezekwem C. A review of the crashworthiness performance of energy absorbing composite structure within the context of materials, manufacturing and maintenance for sustainability. Compos Struct 2021;257(August 2020):113081. https://doi.org/10.1016/j.compstruct.2020.113081.
[7] Cheng P, et al. 3D printed continuous fiber reinforced composite lightweight structures: a review and outlook. Compos B Eng 2023;250(November 2022): 110450. https://doi.org/10.1016/j.compositesb.2022.110450.
[8] Reiner J, Feser T, Waimer M, Poursartip A, Voggenreiter H, Vaziri R. Axial crush simulation of composites using continuum damage mechanics: FE software and material model independent considerations. Compos B Eng 2021;225(September): 109284. https://doi.org/10.1016/j.compositesb.2021.109284.
[9] Abdullah NAZ, Sani MSM, Salwani MS, Husain NA. A review on crashworthiness studies of crash box structure. Thin-Walled Struct 2020;153(July 2019):106795. https://doi.org/10.1016/j.tws.2020.106795.
[10] Boria S, Obradovic J, Belingardi G. Experimental and numerical investigations of the impact behaviour of composite frontal crash structures. Compos B Eng 2015; 79:20–7. https://doi.org/10.1016/j.compositesb.2015.04.016.
[11] Özen İ, Gedikli H, Aslan M. Experimental and numerical investigation on energy absorbing characteristics of empty and cellular filled composite crash boxes. Eng Struct 2023;289(April). https://doi.org/10.1016/j.engstruct.2023.116315.
[12] Saenz-Dominguez I, Tena I, Esnaola A, Sarrionandia M, Torre J, Aurrekoetxea J. Design and characterisation of cellular composite structures for automotive crash-boxes manufactured by out of die ultraviolet cured pultrusion. Compos B Eng 2019; 160(March 2018):217–24. https://doi.org/10.1016/j.compositesb.2018.10.046.
[13] Ciampaglia A, Patruno L, Ciardiello R. Design of a lightweight origami composite crash box: experimental and numerical study on the absorbed energy in frontal impacts. J Compos Sci 2024;8(6). https://doi.org/10.3390/jcs8060224.
[14] Ha NS, Lu G. Thin-walled corrugated structures: a review of crashworthiness designs and energy absorption characteristics. Thin-Walled Structures 2020;157 (April):106995. https://doi.org/10.1016/j.tws.2020.106995.
[15] Zhang J, Karagiozova D, You Z, Chen Y, Lu G. Quasi-static large deformation compressive behaviour of origami-based metamaterials. Int J Mech Sci 2019; 153–154(December 2018):194–207. https://doi.org/10.1016/j.ijmecsci.2019.01.044.
[16] Bandinelli F, Peroni L, Scapin M. Experimental investigation of 3D printed infill structures for crash absorbing applications. Mater Lett 2024;354(October 2023): 135373. https://doi.org/10.1016/j.matlet.2023.135373.
[17] Bouteldja A, Louar MA, Hemmouche L, Gilson L, Miranda-Vicario A, Rabet L. Experimental investigation of the quasi-static and dynamic compressive behavior of polymer-based 3D-printed lattice structures. Int J Impact Eng 2023;180(March). https://doi.org/10.1016/j.ijimpeng.2023.104640.
[18] Andrew JJ, Alhashmi H, Schiffer A, Kumar S, Deshpande VS. Energy absorption and self-sensing performance of 3D printed CF/PEEK cellular composites. Mater Des 2021;208:109863. https://doi.org/10.1016/j.matdes.2021.109863.
[19] Hou W, He P, Yang Y, Sang L. Crashworthiness optimization of crash box with 3D-printed lattice structures. Int J Mech Sci 2023;247(February):108198. https://doi.org/10.1016/j.ijmecsci.2023.108198.
[20] Yang K, Xu S, Zhou S, Xie YM. Multi-objective optimization of multi-cell tubes with origami patterns for energy absorption. Thin-Walled Structures 2018;123(October 2017):100–13. https://doi.org/10.1016/j.tws.2017.11.005.
[21] Sebaey TA, Rajak DKumar, Mehboob H. Internally stiffened foam-filled carbon fiber reinforced composite tubes under impact loading for energy absorption applications. Compos Struct 2021;255(July 2020):112910. https://doi.org/10.1016/j.compstruct.2020.112910.
[22] Um HJ, Lee JS, Shin JH, Kim HS. 3D printed continuous carbon fiber reinforced thermoplastic composite sandwich structure with corrugated core for high stiffness/load capability. Compos Struct 2022;291(December 2021):115590. https://doi.org/10.1016/j.compstruct.2022.115590.

[23] Zhang Y, Cai D, Peng J, Qian Y, Wang X, Miao L. On low-velocity impact behavior of sandwich composites with negative Poisson's ratio lattice cores. Compos Struct 2022;299(January):116078. https://doi.org/10.1016/j.compstruct.2022.116078.
[24] Yan J, et al. Ballistic characteristics of 3D-printed auxetic honeycomb sandwich panel using CFRP face sheet. Int J Impact Eng 2022;164(January):104186. https://doi.org/10.1016/j.ijimpeng.2022.104186.
[25] Acanfora V, Zarrelli M, Riccio A. Experimental and numerical assessment of the impact behaviour of a composite sandwich panel with a polymeric honeycomb core. Int J Impact Eng 2023;171(March 2022):104392. https://doi.org/10.1016/j.ijimpeng.2022.104392.
[26] Ciampaglia A, Fiumarella D, Boursier Niutta C, Ciardiello R, Belingardi G. Impact response of an origami-shaped composite crash box: experimental analysis and numerical optimization. Compos Struct 2021;256(July 2020):113093. https://doi.org/10.1016/j.compstruct.2020.113093.
[27] Bandinelli F, Peroni L, Morena A. Elasto-plastic mechanical modeling of fused deposition 3D printing materials. Polymers 2023;15(1):234. https://doi.org/10.3390/polym15010234.
[28] Bandinelli F, Scapin M, Peroni L. Effects of anisotropy and infill pattern on compression properties of 3D printed CFRP: mechanical analysis and elasto-plastic finite element modelling. Rapid Prototyp J 2024;30(11):142–58. https://doi.org/10.1108/RPJ-11-2023-0385.
[29] Romani A, Perusin L, Ciurnelli M, Levi M. Characterization of PLA feedstock after multiple recycling processes for large-format material extrusion additive manufacturing. Mater Today Sustainab 2024;25(August 2023):100636. https://doi.org/10.1016/j.mtsust.2023.100636.
[30] Copenhaver K, et al. Recyclability of additively manufactured bio-based composites. Compos B Eng 2023;255(August 2022):110617. https://doi.org/10.1016/j.compositesb.2023.110617.
[31] Walker R, et al. Recycling of CF-ABS machining waste for large format additive manufacturing. Compos B Eng 2024;275:111291. https://doi.org/10.1016/j.compositesb.2024.111291.
[32] Bandinelli F, Tito E, Parisi E, Peroni L, Scapin M. Recycling a carbon fiber-reinforced polyamide through 3D printing: a mechanical and physicochemical analysis. Compos B Eng 2025;294. https://doi.org/10.1016/j.compositesb.2025.112147. Apr.
[33] Buj-Corral I, Domínguez-Fernández A, Durán-Llucià R. Influence of print orientation on surface roughness in fused deposition modeling (FDM) processes. Materials (Basel) 2019;12(23):3834. https://doi.org/10.3390/ma12233834.
[34] Golhin AP, Tonello R, Frisvad JR, Grammatikos S, Strandlie A. Surface roughness of as-printed polymers: a comprehensive review, 127. London: Springer; 2023. https://doi.org/10.1007/s00170-023-11566-z.
[35] Ferreira I, Melo C, Neto R, Machado M, Alves JL, Mould S. Study of the annealing influence on the mechanical performance of PA12 and PA12 fibre reinforced FFF printed specimens. Rapid Prototyp J 2020;26(10):1761–70. https://doi.org/10.1108/RPJ-10-2019-0278.
[36] Bu H, et al. Enhanced interlayer strength in 3D-printed PA12 composites via electromagnetic induction post-processing. Addit Manuf 2024;92(August):104383. https://doi.org/10.1016/j.addma.2024.104383.
[37] Peroni M, Peroni L, Avalle M. High strain-rate compression test on metallic foam using a multiple pulse SHPB Apparatus. Journal De Physique 2006;134:609–16. https://doi.org/10.1051/jp4:2006134094. *IV : JP*.
[38] Bussac MN, Collet P, Gary G, Othman R. An optimisation method for separating and rebuilding one-dimensional dispersive waves from multi-point measurements. Application to elastic or viscoelastic bars. J Mech Phys Solids 2002;50(2):321–49. https://doi.org/10.1016/S0022-5096(01)00057-6.
[39] Pochhammer Von Herrn L. Ueber die Fortpflanzungsgeschwindigkeiten kleiner Schwingungenin einem unbegrenzten isotropen kreiscylinder. J Reine Angew Math 1876;81.
[40] Chree C. The equations of an isotropic elastic solid in polar and cylindrical Co-ordinates, their solution and application. Trans Cambridge Philos Soc 1887;14:250–369.
[41] Duan Y, Du B, Shi X, Hou B, Li Y. Quasi-static and dynamic compressive properties and deformation mechanisms of 3D printed polymeric cellular structures with Kelvin cells. Int J Impact Eng 2019;132(May). https://doi.org/10.1016/j.ijimpeng.2019.05.017.
[42] Mamalis AG, Manolakos DE, Ioannidis MB, Papapostolou DP. On the response of thin-walled CFRP composite tubular components subjected to static and dynamic axial compressive loading: experimental. Compos Struct 2005;69(4):407–20. https://doi.org/10.1016/j.compstruct.2004.07.021.
[43] Zhou J, Guan Z, Cantwell WJ. The energy-absorbing behaviour of composite tube-reinforced foams. Compos B Eng 2018;139(December 2017):227–37. https://doi.org/10.1016/j.compositesb.2017.11.066.
[44] Duan Y, et al. Effects of cell size vs. cell-wall thickness gradients on compressive behavior of additively manufactured foams. Compos Sci Technol 2020;199(July):108339. https://doi.org/10.1016/j.compscitech.2020.108339.
[45] Gibson LJ. Biomechanics of cellular solids. J Biomech 2005;38(3):377–99. https://doi.org/10.1016/j.jbiomech.2004.09.027.
[46] Feng G, Li S, Xiao L, Song W. Mechanical properties and deformation behavior of functionally graded TPMS structures under static and dynamic loading. Int J Impact Eng 2023;176(March):104554. https://doi.org/10.1016/j.ijimpeng.2023.104554.
[47] Andrew JJ, Schneider J, Ubaid J, Velmurugan R, Gupta NK, Kumar S. Energy absorption characteristics of additively manufactured plate-lattices under low-velocity impact loading. Int J Impact Eng 2021;149(August 2020):103768. https://doi.org/10.1016/j.ijimpeng.2020.103768.
[48] Sun G, Li S, Liu Q, Li G, Li Q. Experimental study on crashworthiness of empty/aluminum foam/honeycomb-filled CFRP tubes. Compos Struct 2016;152:969–93. https://doi.org/10.1016/j.compstruct.2016.06.019. Sep.
[49] Langseth M, Hopperstad O. Static and dynamic axial crushing of square thin-walled aluminium extrusions. Int J Impact Eng 1996;18(7–8):949–68. https://doi.org/10.1016/S0734-743X(96)00025-5. nosMay.
[50] Wang Y, Li X, Chen Y, Zhang C. Strain rate dependent mechanical properties of 3D printed polymer materials using the DLP technique. Addit Manuf 2021;47(September):102368. https://doi.org/10.1016/j.addma.2021.102368.
[51] Vidakis N, Petousis M, Velidakis E, Liebscher M, Mechtcherine V, Tzounis L. On the strain rate sensitivity of fused filament fabrication (Fff) processed pla, abs, petg, pa6, and pp thermoplastic polymers. Polymers (Basel) 2020;12(12):1–15. https://doi.org/10.3390/polym12122924.
[52] Morano C, Alfano M, Pagnotta L. Effect of strain rates and heat exposure on polyamide (PA12) processed via selective laser sintering. Materials (Basel) 2023;16(13). https://doi.org/10.3390/ma16134654.
[53] Sun ZP, Guo YB, Shim VPW. Influence of printing direction on the dynamic response of additively-manufactured polymeric materials and lattices. Int J Impact Eng 2022;167(May):104263. https://doi.org/10.1016/j.ijimpeng.2022.104263.
[54] Fíla T, et al. Impact testing of polymer-filled auxetics using split Hopkinson pressure bar. Adv Eng Mater 2017;19(10):1–13. https://doi.org/10.1002/adem.201700076.
[55] Sun ZP, Guo YB, Shim VPW. Static and dynamic crushing of polymeric lattices fabricated by fused deposition modelling and selective laser sintering – an experimental investigation. Int J Impact Eng 2022;160(October 2021):104059. https://doi.org/10.1016/j.ijimpeng.2021.104059.
[56] Rapaka SD, Pandey M, Annabattula RK. Dynamic compressive behaviour of auxetic and non-auxetic hexagonal honeycombs with entrapped gas. Int J Impact Eng 2020;146(June):103718. https://doi.org/10.1016/j.ijimpeng.2020.103718.
[57] Feng H, Liu L, Zhao Q. Experimental and numerical investigation of the effect of entrapped air on the mechanical response of Nomex honeycomb under flatwise compression. Compos Struct 2017;182(September):617–27. https://doi.org/10.1016/j.compstruct.2017.09.080.
[58] Sun Y, Li QM. Effect of entrapped gas on the dynamic compressive behaviour of cellular solids. Int J Solids Struct 2015;63:50–67. https://doi.org/10.1016/j.ijsolstr.2015.02.034.
[59] Hosur MV, Alexander J, Jeelani S, Vaidya UK, Mayer A. High strain compression response of affordable woven carbon/epoxy composites. J Reinf Plast Compos 2003;22(3):271–96. https://doi.org/10.1177/0731684403022003844.
[60] Fu J, Liu Q, Ma X, Cai M. Energy absorption characteristics of bio-inspired multi-corner CFRP tubes under axial quasi-static and dynamic loading. Thin-Walled Structures 2024;205(PB):112551. https://doi.org/10.1016/j.tws.2024.112551.